Electronic Supplementary Information

Rational Design of 3D Inverse Opals Heterogeneous Composites Microspheres as Excellent Visible-Light-Induced NO_2 Sensor at Room Temperature

Tianshuang Wang, Qi Yu, Sufang Zhang, Xueying Kou, Peng Sun* and Geyu Lu*

State Key Laboratory on Integrated Optoelectronics, College of Electronic Science and Engineering, Jilin University, 2699 Qianjin Street, Changchun 130012, People's Republic of China.

Corresponding Authors: Tel: +86-431-85167808; Fax: +86-431-86167808.
E-mail addresses: pengsun@jlu.edu.cn (Peng Sun); lugy@jlu.edu.cn (Geyu Lu).

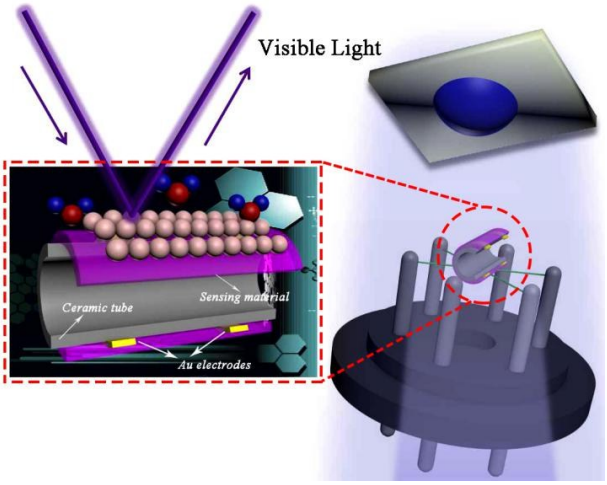

Figure S1. The detailed schematic of gas sensor instrument.

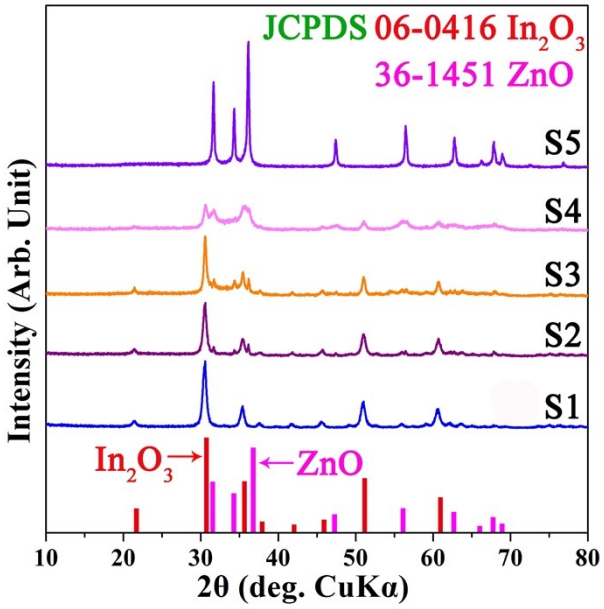

Figure S2. XRD patterns of the as-prepared S1-S5 samples.

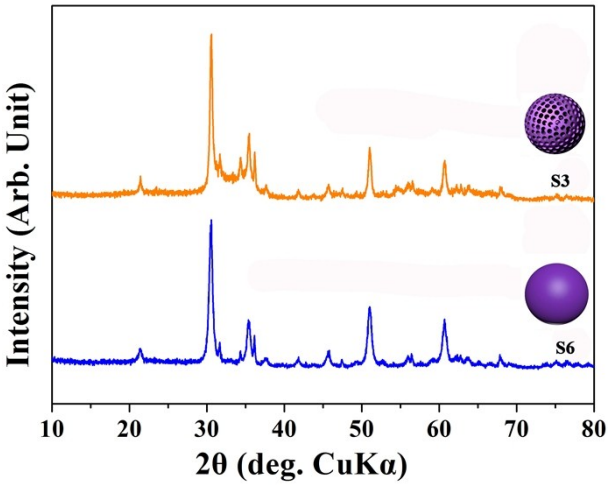

Figure S3. XRD patterns of the as-prepared S3 and S6 samples.

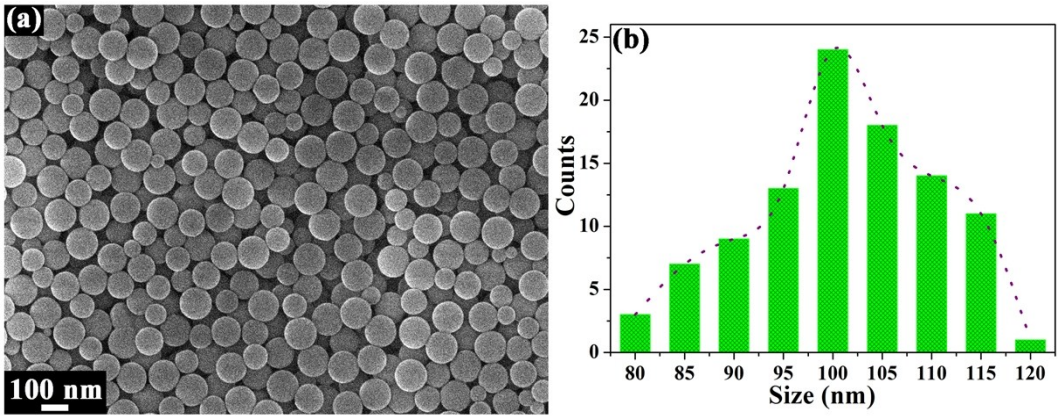

Figure S4. (a) Scanning electron microscopy (SEM) image and (b) the size distribution histogram of the S-PS spheres.

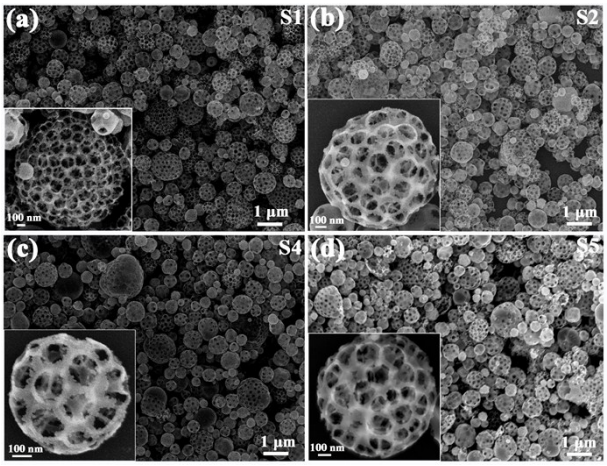

Figure S5. Typical SEM images of the as-prepared products (a) 3D IO In_2O_3 microspheres (S1 sample), (b and c) 3D IO In_2O_3-ZnO HCMs (S2 and S4 samples), (d) 3D IO ZnO microspheres (S5 sample).

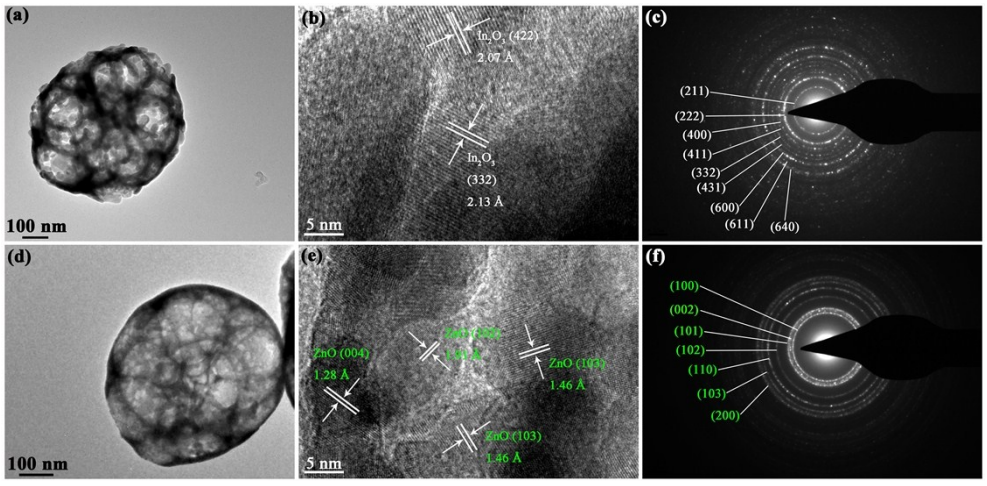

Figure S6. TEM images of (a) S1 and (d) S5 samples; HRTEM images of (b) S1 and (e) S5 samples; SAED patterns of (c) S1 and (f) S5 samples.

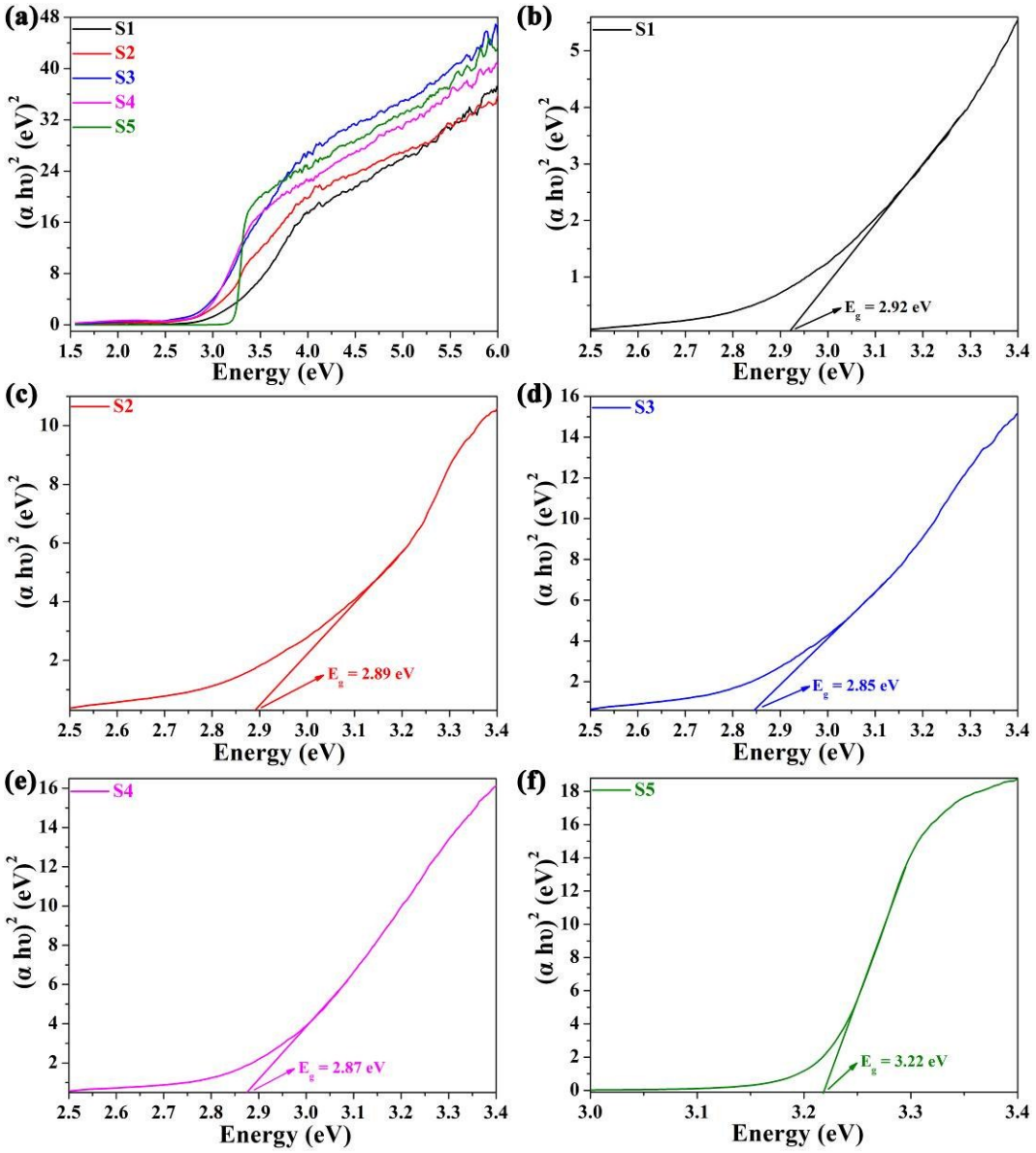

Figure S7. (a-f) The estimated band gap energy of 3D IO In_2O_3-ZnO HCMs with different component ratios (S1-S5 samples).

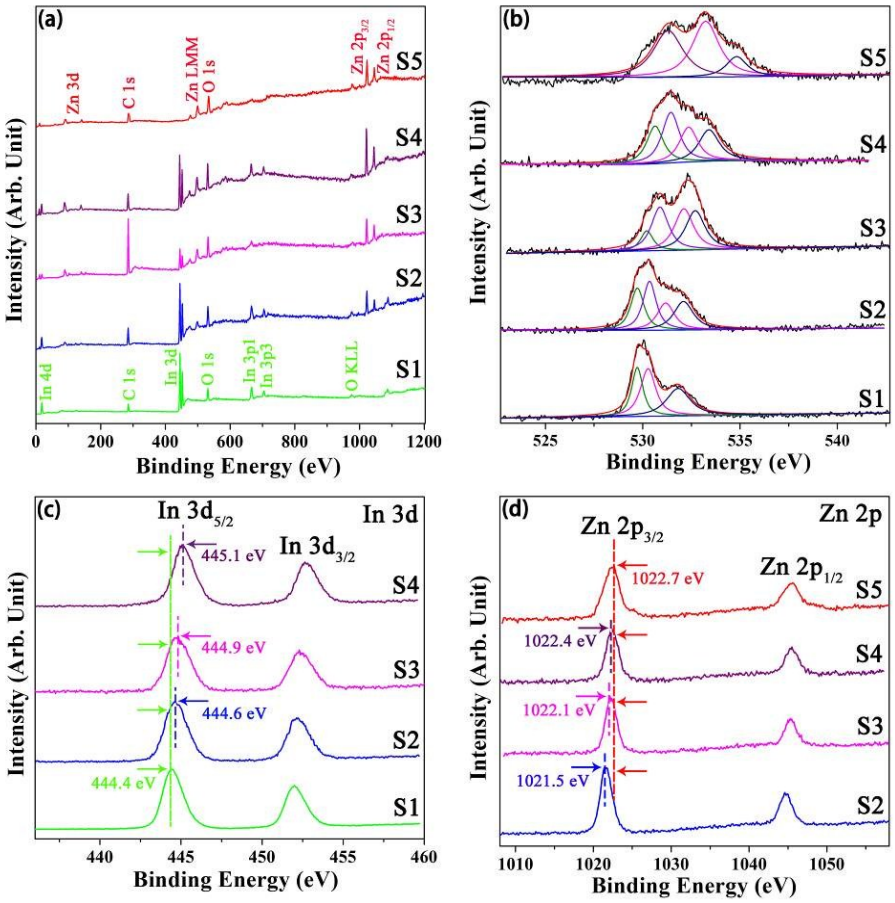

Figure S8. (a) The complete XPS spectra and (b) the corresponding enlarged O 1s XPS spectra of S1-S5 samples, the detailed XPS spectra of (c) In 3d core level region of S1-S4 samples and (d) Zn 2p core level region of S2-S5 samples.

The X-ray photoelectron spectroscopy (XPS) was used to investigate the surface elemental composition and chemical status of the as-prepared S1-S5 samples (**Figure S8**). In the full range spectra Figure S8(a), peaks corresponding to C, O, In and/or Zn were clearly observed in different samples, and no impurities could be found. The O 1s XPS spectra of various samples were enlarged in Figure S8(b). Accordingly, the O 1s peaks of the S1 and S5 samples were both fitted to three peaks by Gaussian simulation peaks, which could be attributed to three kinds of oxygen species: the lattice oxygen O_L in crystalline In_2O_3 (529.7 eV) and ZnO (530.3 eV), the middle of the three curves is O_V component in oxygen vacancy regions, and the O_C component is assigned to chemisorbed or dissociated oxygen or -OH species, respectively. The samples (S2-S4) all displayed four peaks due to different chemical environment of O in composite oxides, each characteristic peak had some shift. The four peaks located at around 530, 530.9, 531.9 and 532.7 eV, respectively. Accordingly, the In 3d high-resolution XPS spectra of S1-S4 samples can be observed in Figure S8(c). For S1 sample, the two strong peaks centered at 444.4 and 452 eV correspond to the In $3d_{5/2}$ and In $3d_{3/2}$, respectively. The Zn 2p high-resolution XPS spectra (Figure S8(d)) in S2-S5 samples showed two symmetric peaks with the same spin-orbit splitting (~23eV), and the peaks around 1022.7 eV and 1045.6 eV confirmed the presence of Zn $2p_{3/2}$ and Zn$2p_{1/2}$ peaks, respectively. Compared to pure In_2O_3 and ZnO, with the increasing amount of the other materials in the In_2O_3-ZnO heterogeneous composites samples, the binding energy of the In 3d ($3d_{5/2}$ and $3d_{3/2}$) gradually shifted to higher binding energy, and the binding energy of the Zn 2p ($2p_{3/2}$ and $2p_{1/2}$) gradually shifted to lower binding energy. This could be attributed to the electronic interactions that existed between the components in the heterogeneous composites. As well due to more majority carriers may be transferred, the shift degree of the In 3d or Zn 2p spectrum in the In_2O_3-ZnO heterogeneous composites will become more obvious.

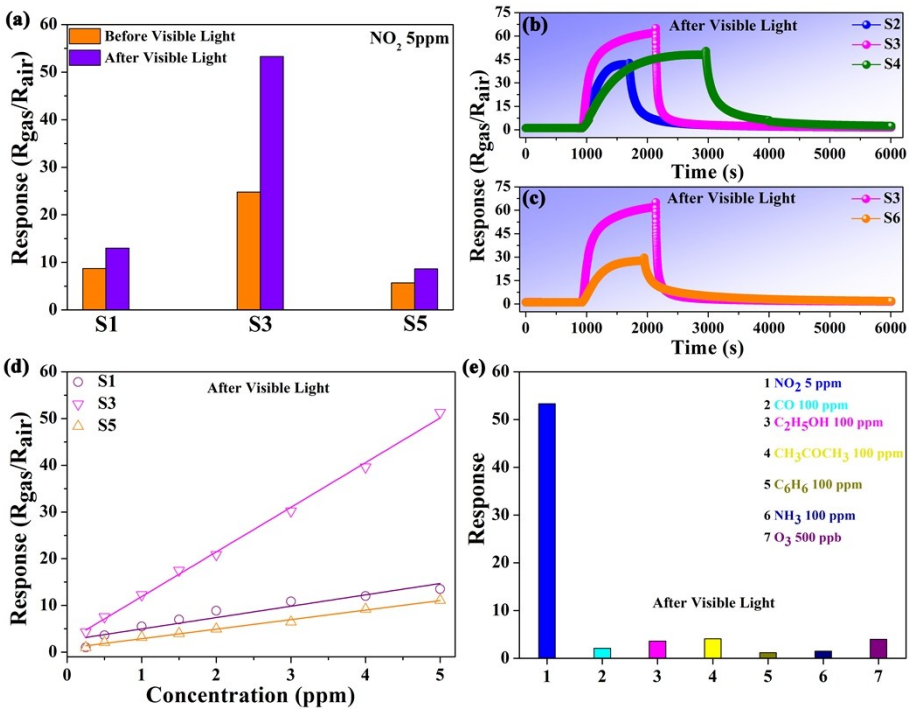

Figure S9. (a) The gas responses of the S1, S3 and S5 sensors toward 5 ppm NO_2 before and after visible light. (b) Gas sensing transients of the S2-S4 sensors when exposed to 5 ppm of NO_2 after visible light. (c) The gas sensing transients of S3 and S6 at room temperature under visible light irradiation. (d) Responses vs NO_2 concentration for the S1, S3 and S5 sensors under visible light irradiation. (e) Selectivity of the S3 sensor to various gases under visible light irradiation.

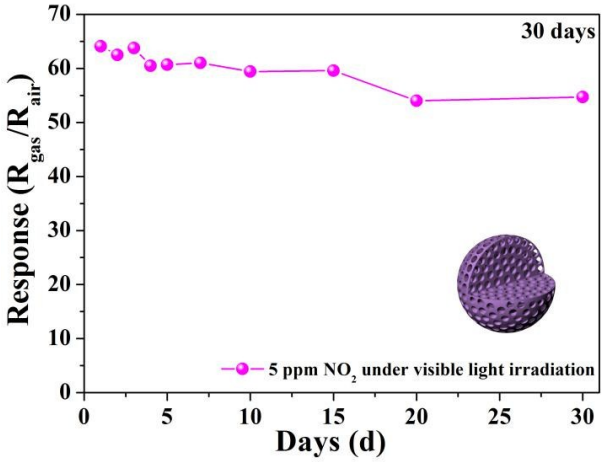

Figure S10. Long-term stability of the gas sensor based on the S3 sample.

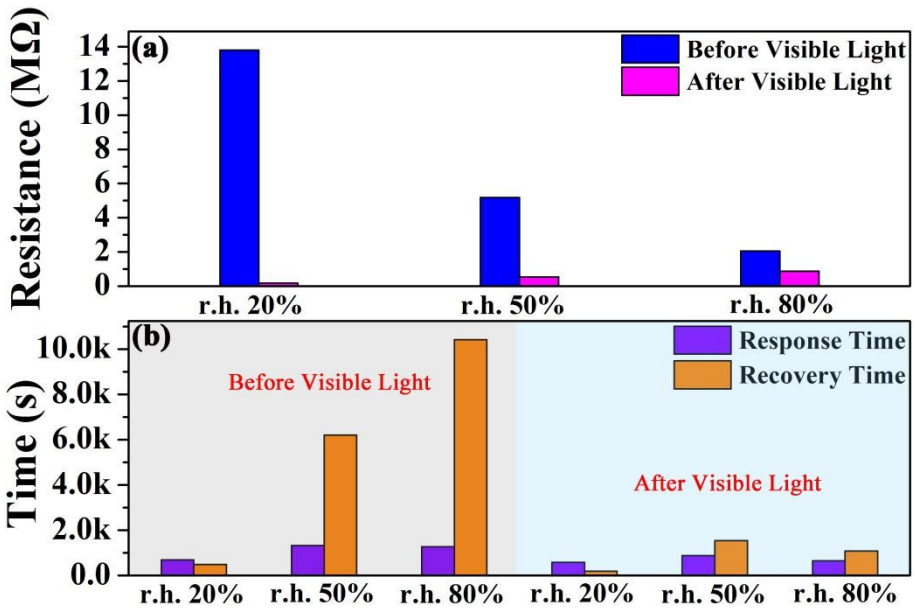

Figure S11. (a) The resistance in air (R_a) of the S3 sensor with various relative humidity (r.h. = 20%, 50% and 80%) at room temperature (25 °C) before and after visible light. (b) Relative humidity vs. response and recovery times plots at 25 °C for the S3 sensor.

Table S1. Comparison of gas sensing performances of some room-temperature NO_2 gas sensors.

Materials	Methods	Concentration [ppm]	NO_2 response [R_{gas}/R_{air}]	Recovery time [s]	Light sources
ZnO[1]	Gravity deposition	1	2.5	40	UV light
ZnO[2]	Suspension flame spraying	1	3.6	480	Visible light
ZnO[3]	Gravity deposition	1	3	---	UV light
ZnO/In_2O_3[4]	Co-precipitation	5	2.2	695	UV light
CdS/ZnO[5]	Hydrothemal	1	4.5	227	Visible light
This work	USP	1	12.3	215	Visible light

References

1. X. S. Su, L. Gao, F. Zhou, W. P. Cai and G. T. Duan, “Close network” effect of a ZnO micro/nanoporous array allows high UV-irradiated NO_2 sensing performance, RSC Adv., **2017**, 7 (34), 21054.
2. X. Geng, C. Zhang, Y. F. Luo and M. Debliquy, Flexible NO_2 gas sensors based on sheet-like hierarchical ZnO_{1-x} coatings deposited on polypropylene papers by suspension flame spraying, J. Taiwan Inst. Chem. E., **2017**, 75, 280.
3. X. S. Su, G. T. Duan, Z. K. Xu, F. Zhou and W. P. Cai, Structure and thickness-dependent gas sensing responses to NO_2 under UV irradiation for the multilayered ZnO micro/nanostructured porous thin films, J. Colloid Interf. Sci., **2017**, 503, 150.
4. E. Espid, F. Taghipour, Development of highly sensitive ZnO/In_2O_3 composite gas sensor activated by UV-LED. Sens. Actuators B, **2017**, 241, 828.
5. Z. Yang, L. J. Guo, B. Y. Zu, Y. N. Guo, T. Xu and X. C. Dou, CdS/ZnO core/shell nanowire-built films for enhanced photodetecting and optoelectronic gas-sensing applications, Adv. Optical Mater., **2014**, 2, 738.